Reprinted from JOURNAL OF THE OPTICAL SOCIETY OF AMERICA, Vol. 53, No. 7, 816–821, July 1963
Printed in U. S. A.

Radiant Emission Characteristics of Diffuse Conical Cavities

E. M. SPARROW AND V. K. JONSSON
Heat Transfer Laboratory, Department of Mechanical Engineering, University of Minnesota, Minneapolis, Minnesota

(Received 10 September 1962)

The radiant interchange within a diffuse conical cavity has been formulated without approximation for both cases of prescribed wall temperature and prescribed wall heat flux. Highly accurate numerical solutions have been obtained for a wide range of cone opening angles and surface emissivities. Results are presented for the radiant efflux from the cavity as a whole and also for the distributions along the cavity surface of such quantities as the apparent radiant emittance, local heat flux (for prescribed surface temperature), and temperature (for prescribed heat flux). A comparison with the approximate analysis of Gouffe disclosed large errors in this prior work.

INTRODUCTION

THE radiant emission of cavities has been a subject of common interest to investigators of illumination and of radiative heat transfer. This interest stems from the fact that a cavity may serve as a source of radiant energy having considerably higher emissive power than a plane surface. This property is sometimes referred to as the cavity effect and is related to the multiple reflections which are sustained by rays before they stream out of the cavity.

A useful survey of analytical work on cavity-type sources of radiant energy has been presented in Ref. 1. In discussing the various investigations, care was taken to bring out the approximations which were made in each; and it was indicated that certain approximations were of doubtful validity. Meanwhile, in the heat-transfer literature, various studies of the emission characteristics of diffusely emitting and reflecting cavities have been carried out without approximation. Results have been presented for the circular cylinder, the sphere, and the parallel-walled groove.[2] A new formulation for radiant interchange within a diffusely emitting but specularly reflecting cylinder has been devised,[3] but this has yet to be applied to a finite-length cavity.

An important cavity configuration for which there exists neither a correct formulation nor reliable numerical results is the diffuse conical cavity. It is the aim of this report to treat the diffuse conical cavity without approximation. An exact, systematic formulation is presented and from this there are obtained numerical results for both the over-all and local radiant energy transfers. The over-all results correspond to the radiant energy flux streaming out of the cavity as a whole, while the local results relate to the radiant energy fluxes which leave various surface locations within the cavity. This information is provided for a wide range of cone opening angles and radiation properties of the cavity surface. The analysis and results include both cases of uniform surface temperature and uniform surface heat flux. Within the knowledge of the authors, the latter of these boundary conditions has not previously been considered in cavity studies. The only prior work known to the authors[4,5] on the diffuse conical cavity is due to Gouffe.[6] As discussed in Ref. 1, Gouffe treated the cone, among other configurations, within the framework of a highly approximate theory. Results of uncertain accuracy were reported for the effective emissivity of the cavity (i.e., over-all energy flux streaming from the cavity). These results will be compared later with those of the present analysis, and substantial errors will be demonstrated. Gouffe's method did not provide any information on the distribution of the radiant flux along the walls of the cavity.

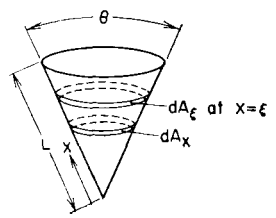

FIG. 1. Schematic of a conical cavity.

A schematic diagram of the cavity under study is shown in Fig. 1. The cone opening angle is θ, while L is the slant height of the cavity. The coordinate x measures distances along the surface from the apex. In the analysis that follows, the cavity surface is assumed to emit and reflect diffusely, i.e., Lambert's cosine law is obeyed.

ANALYSIS

The first step in the analysis is to write a radiant flux balance for a typical surface element on the wall of the cavity. For this purpose it is convenient to select a ring-shaped area dA_x as shown in Fig. 1. If energy conservation is to be satisfied, the radiant flux streaming away from the area element must equal the sum of the emitted energy plus the reflected portion of the incident energy. The radiant energy leaving an

[1] C. S. Williams, J. Opt. Soc. Am. **51**, 566 (1961).
[2] E. M. Sparrow, L. U. Albers, E. R. G. Eckert, V. K. Jonsson, and J. L. Gregg, J. Heat Transfer **C84**, 73, 188, 270 (1962).
[3] K. S. Krishnan, Proc. Roy. Soc. (London) **A257**, 302 (1960).
[4] During the review by the papers committee, unpublished analytical work by Page (Ref. 5) on the cone problem was brought to the attention of the authors, who wish to acknowledge it here.
[5] C. H. Page, National Bureau of Standards (private communication, 1963).
[6] A. Gouffe, Rev. Opt. Nos. 1–3 (1945).

element per unit time and area has been variously called the apparent radiant emittance, the radiosity, the brightness, or the total emission. It is denoted here by the symbol B. The incident energy per unit time and area, the irradiance, is denoted by I. Then, from energy conservation

$$B(x)=\epsilon\sigma T^4(x)+\rho I(x), \tag{1}$$

in which the possible dependence of B, T, and I on x is indicated explicitly, and ϵ and ρ, respectively, represent the emissivity and reflectivity.

The next step is to eliminate the irradiance I from Eq. (1). This may be done by taking cognizance of the fact that radiant energy arriving at dA_x must come from other surface locations on the cavity wall.[7] For instance, consider the radiation leaving some other surface location $x=\xi$ (see Fig. 1). An amount $B(\xi)dA_\xi$ leaves dA_ξ in all directions. Of this a quantity $[B(\xi)dA_\xi]dF_{\xi-x}$ arrives at dA_x, where $dF_{\xi-x}$ is a geometrical factor[8] for diffuse interchange between surface elements dA_ξ and dA_x. Utilizing the reciprocity theorem for diffuse geometrical factors, which states (Ref. 9, p. 9)

$$dA_\xi dF_{\xi-x}=dA_x dF_{x-\xi}, \tag{2}$$

it follows that the radiant energy leaving dA_ξ and arriving at dA_x is $B(\xi)dF_{x-\xi}dA_x$; or, per unit area at dA_x, this is $B(\xi)dF_{x-\xi}$. But, energy arrives at x from all locations $0\leq\xi\leq L$, and the total is found by integration:

$$I(x)=\int_{\xi=0}^{L} B(\xi)dF_{x-\xi}. \tag{3}$$

Introducing this into the radiant flux balance (1), there follows

$$B(x)=\epsilon\sigma T^4(x)+\rho\int_{\xi=0}^{L} B(\xi)dF_{x-\xi}. \tag{4}$$

In general, the reflectivity $\rho=1-\alpha$ for an opaque surface, in which α is the absorptivity. Further, for a gray surface, $\alpha=\epsilon$ and $\rho=1-\epsilon$. The graybody postulate will be employed in the subsequent analysis.

Inspection of Eq. (4) reveals that the unknown brightness distribution B appears under the integral sign as well as in other parts of the equation. Therefore, Eq. (4) is an integral equation. The $B(x)$ and $B(\xi)$ are the same functions; only the names of the independent variables have been interchanged. To proceed with a solution of Eq. (4), it remains to provide the thermal boundary conditions and to derive the angle factor $dF_{x-\xi}$.

[7] Energy entering the cavity from outside is generally not included in studies of the emission characteristics of cavities.

[8] The geometrical factor represents the fraction of the radiant energy leaving one surface element which arrives at another surface element.

[9] M. Jakob, *Heat Transfer* (John Wiley & Sons, Inc., New York, 1957), Vol. 2.

Uniform Wall Temperature

When the surface of the cavity is at uniform temperature, $T(x)$ is replaced by T_w (a constant), and Eq. (4) is rewritten as

$$\epsilon_a(x)=\epsilon+(1-\epsilon)\int_{\xi=0}^{L}\epsilon_a(\xi)dF_{x-\xi}, \tag{5}$$

in which ϵ_a is a ratio of the apparent radiant emittance to the blackbody emissive power, i.e.,

$$\epsilon_a(x)=B(x)/\sigma T_w^4. \tag{6}$$

ϵ_a may be logically regarded as the local apparent emissivity. Since the integral appearing on the right-hand side of Eq. (5) is always positive, it follows that ϵ_a is always greater than ϵ.

For problems in illumination or in pyrometry, the local apparent emissivity is itself of substantial interest. Additionally of interest are the heat-transfer characteristics of the cavity. The net local rate of heat transfer per unit area, denoted by q, is the difference between the radiant flux emitted at a surface location and that which is absorbed,

$$q(x)=\epsilon\sigma T^4(x)-\alpha I(x). \tag{7a}$$

Utilizing Eq. (1), this becomes

$$q(x)=[\epsilon/(1-\epsilon)][\sigma T^4(x)-B(x)]; \tag{7b}$$

and, for the case of uniform wall temperature,

$$\frac{q(x)}{\sigma T_w^4}=\frac{\epsilon}{1-\epsilon}\left[1-\frac{B(x)}{\sigma T_w^4}\right]=\frac{\epsilon}{1-\epsilon}[1-\epsilon_a(x)]. \tag{8}$$

Thus, it is seen that the local heat flux $q(x)$ and the apparent radiant emittance $B(x)$ (or the apparent emissivity ϵ_a) are essentially interchangeable quantities.

The rate Q at which radiant energy streams outward through the cavity opening is found by integrating the local heat flux q over the area of the cavity wall.

$$Q=\int_0^L q(x)2\pi x\sin(\theta/2)dx,$$

or

$$\frac{Q}{\sigma T_w^4 A_0}=\frac{2}{\sin(\theta/2)}\int_0^1\frac{q(x)}{\sigma T_w^4}\frac{x}{L}d\left(\frac{x}{L}\right), \tag{9}$$

in which A_0 is the area of the cavity opening $A_0=\pi L^2\sin^2(\theta/2)$. As written, the second member of Eq. (9) compares the radiant flux Q which passes through the cavity opening with that from a blackbody stretched across the opening. This represents the hemispherical emissivity of the cavity as a whole. If there were no cavity, $Q/\sigma T_w^4 A_0$ would equal ϵ. Due to the presence of the cavity, this ratio will exceed ϵ. Therefore, the deviation from ϵ of $Q/\sigma T_w^4 A_0$ provides a measure of the cavity effect.

It is easily seen that the results for $B(x)$ or $\epsilon_a(x)$, $q(x)$, and Q all depend upon the solution of the integral equation (5). These solutions and the corresponding results are discussed later.

Uniform Wall Heat Flux

When the wall heat flux is prescribed, the quantities of practical interest which remain to be determined are the apparent radiant emittance $B(x)$ and the temperature distribution $T(x)$ along the cavity surface. For the case of uniform wall heat flux, $q(x)$ is replaced by q_w (a constant) and Eq. (7b) is solved for $\sigma T^4(x)$;

$$\sigma T^4(x)=[(1-\epsilon)/\epsilon]q_w+B(x). \tag{10}$$

Eliminating $\sigma T^4(x)$ between Eqs. (10) and (4), there is obtained

$$\beta(x)=1+\int_{\xi=0}^{L}\beta(\xi)dF_{x-\xi};\quad \beta=\frac{B}{q_w}. \tag{11}$$

The foregoing is an integral equation of the same general type as has already been encountered in Eq. (5). However, there is an interesting difference in detail; namely, that the surface emissivity ϵ, which appears as a parameter in Eq. (5), is absent in Eq. (11).

Clearly, once solutions of Eq. (11) have been found, then both the apparent radiant emittance and the surface temperature distributions will be known. These solutions and results are given in a later section.

Geometrical Factor Derivation

A necessary ingredient for the foregoing analysis is the geometrical factor for diffuse interchange between two ring-shaped area elements respectively located at positions $x=x$ and $x=\xi$ on the cavity wall (see Fig. 1). The derivation of this geometrical factor[10-12] facilitated by first considering the interchange between two coaxial, parallel circular disks of radii r_1 and r_2 which are separated by a distance h. The angle factor for disk-to-disk interchange, F_{d-d}, which gives the fraction of the radiant energy leaving Disk 1 which arrives at Disk 2 is (Ref. 9, p. 14)

$$F_{d-d}=\{h^2+r_1^2+r_2^2-[(h^2+r_1^2+r_2^2)^2-4r_1^2r_2^2]^{\frac{1}{2}}\}/2r_1^2. \tag{12}$$

Now, let the disks share a common axis with the conical cavity, and let Disk 1 be stretched across the cavity at location $x=\xi$ and Disk 2 be stretched across the cavity at location $x=x$. Then,

$$r_1=\xi\sin(\theta/2),\qquad r_2=x\sin(\theta/2),\qquad h=|\xi-x|\cos(\theta/2).$$

With these, Eq. (12) becomes

$$F_{d-d}(\xi,x)=\frac{x^2+\xi^2-2x\xi\cos^2(\theta/2)-|\xi-x|[(x+\xi)^2-4x\xi\cos^2(\theta/2)]^{\frac{1}{2}}}{2\xi^2\sin^2(\theta/2)}. \tag{13}$$

Also, consider the interchange between a disk located at $x=\xi$ and another disk located at $x=x+dx$. The appropriate disk-to-disk geometrical factor $F_{d-d}(\xi, x+dx)$ is identical to Eq. (13), with x replaced by $x+dx$.

Suppose for concreteness that $\xi>x$. From physical reasoning, it is easy to see that energy leaving the disk at ξ and passing through a transparent disk at $x+dx$ must either strike a disk at x or else be incident on a ring element of length dx (area dA_x) on the surface of the cone, therefore

$$F_{d-d}(\xi, x+dx)=F_{d-d}(\xi,x)+dF_{d-r}(\xi,x), \tag{14}$$

where the subscript $d-r$ indicates interchange between disk and ring. After rearranging Eq. (14), there is obtained

$$dF_{d-r}(\xi,x)=(\partial F_{d-d}/\partial x)dx. \tag{15}$$

Alternatively, by the reciprocity theorem, the geometrical factor from a ring at x to a disk at ξ is

$$F_{r-d}(x,\xi)=[\xi^2\sin(\theta/2)/2x](\partial F_{d-d}/\partial x). \tag{16}$$

Also, the geometrical factor for interchange between a ring at x and a disk at $\xi+d\xi$, $F_{r-d}(x, \xi+d\xi)$, is identical to Eq. (16) with ξ replaced by $\xi+d\xi$.

It is further evident that radiant energy leaving a ring at x and passing through a transparent disk at ξ must either strike a disk at $\xi+d\xi$ or else be incident on a ring element of length $d\xi$ (area dA_ξ) on the surface of the cone, thus

$$F_{r-d}(x,\xi)=F_{r-d}(x, \xi+d\xi)+dF_{r-r}(x,\xi), \tag{17}$$

where the subscript $r-r$ denotes ring-to-ring interchange. But, $dF_{r-r}(x,\xi)$ is precisely the geometrical factor $dF_{x-\xi}$ which has appeared in the integral equations (5) and (11), and so

$$dF_{x-\xi}=-\frac{\partial F_{r-d}}{\partial\xi}d\xi=-\frac{\sin(\theta/2)}{2x}\frac{\partial}{\partial\xi}\left[\xi^2\frac{\partial F_{d-d}}{\partial x}\right]d\xi. \tag{18}$$

The desired geometrical factor is obtained by a double differentiation of the disk-to-disk relation (13), with proper cognizance given to the absolute magnitude

[10] This method of analysis has been employed in Refs. 11 and 12.
[11] A. C. Bartlett, Phil. Mag. Suppl. 6, 40, 111 (1920).
[12] H. Buckley, Phil. Mag. Suppl. 7, 4, 753 (1927).

sign. From this, there results after rearrangement

$$dF_{x-\xi}=\frac{\cos^2(\theta/2)}{2x\sin(\theta/2)}\times\left\{1-|\xi-x|\frac{(\xi-x)^2+6\xi x\sin^2(\theta/2)}{[(\xi-x)^2+4\xi x\sin^2(\theta/2)]^{\frac{3}{2}}}\right\}d\xi. \quad (19)$$

Inspection of the foregoing reveals that the cone opening angle θ appears as a parameter in the geometrical factor expression. Correspondingly, the solutions of the integral equations (5) and (11) will also depend upon parametric values of θ. It is interesting to observe that when $\theta\rightarrow 0$ Eq. (19) reduces to the geometrical factor between two ring elements on the surface of a circular cylinder. In the limit when $\theta\rightarrow 0$, $x\sin(\theta/2)\rightarrow r$ and $\xi\sin(\theta/2)\rightarrow r$, where r is the radius of the cylinder.

With the geometrical factor thus derived, solutions of the governing equations can now be discussed.

Solutions

A detailed study of the governing integral equations (5) and (11) and the geometrical factor expression (19) reveals that closed-form, analytical solutions are not possible. However, with the aid of modern electronic computing equipment, it is possible to obtain highly accurate numerical solutions. In the case of Eq. (5) it is necessary to specify two parameters, the angle θ and the emissivity ϵ, for each solution; while for Eq. (11), the angle θ is the only parameter.

The numerical solutions were carried out by an iterative procedure. Considering Eq. (5), the first step was to specify the values of θ and ϵ. Then, a trial distribution for $\epsilon_a(\xi)$ was proposed. For a fixed value of x, the integration in ξ which appears on the right side of Eq. (5) could be carried out numerically. This yielded a value of ϵ_a corresponding to the fixed x value. Then, another value of x was selected, the integration repeated, and an ϵ_a corresponding to the second x value obtained. By applying this procedure at every mesh point x in the range $0\leq x\leq L$, a new ϵ_a distribution was generated. This new ϵ_a distribution was then used as input to the right side of Eq. (5) and the aforementioned operations repeated. This was continued until convergence was achieved.

The numerical integrations were performed using Simpson's rule. In carrying out the integration, it was necessary to take cognizance of the fact that the geometrical factor has a discontinuous slope at $x=\xi$; note the absolute magnitude signs in Eq. (19). Accurate results cannot be obtained by numerically integrating across such a discontinuity. Rather, the integration has to be performed separately on each side of the discontinuity (i.e., from $x=0$ to $x=\xi$ and then from $x=\xi$ to $x=L$). This causes some complication, since the conventional Simpson's rule can only be applied to an odd number of points, while the separate integrations noted above would sometimes have to be extended over an even number of points. This difficulty was circumvented and accuracy simultaneously improved by interpolating between the unknown values of ϵ_a. Quadratic interpolation was used which has the same truncation error as the Simpson's rule integration. The step size for the integration was selected so that there would be 51 unknown values of ϵ_a in the range $0\leq x/L\leq 1$; however, the integrations were extended over 101 points because of the interpolation noted above. Thus, a very small step size was used and, consequently, the results are believed to be highly accurate.

Similar remarks apply to the solution of Eq. (11).

RESULTS

Uniform Wall Temperature

The governing equation (5) for uniform wall temperature has been solved for cone-opening angles θ of 30°, 60°, 90°, and 120° and for surface emissivities ϵ of 0.3, 0.5, 0.7, and 0.9. The solutions have been utilized in conjunction with Eq. (9) to calculate the rate Q at which radiant energy streams outward from the cavity opening. The results thus obtained have been plotted as solid lines in Fig. 2. The curves have been extended over the entire range of opening angles from 0° to 180°. The limiting values for $\theta=0°$ and 180° were found as follows: First, as θ approaches 0°, it may be noted that the cone will approach a circular cylinder of large length-to-diameter ratio. Results for the long cylinder were available from previously referenced work (Ref. 2, p. 73). Second, as θ approaches 180°, the conical cavity approaches a plane surface. Correspondingly, the radiant interaction between surface elements of the cavity vanishes, and $Q/A_0\sigma T_w^4$ approaches ϵ.

As already noted, $A_0\sigma T_w^4$ represents the emission of a black surface having the same area as the cavity opening, and therefore, $Q/A_0\sigma T_w^4$ represents an apparent hemispherical emissivity of the cavity as a

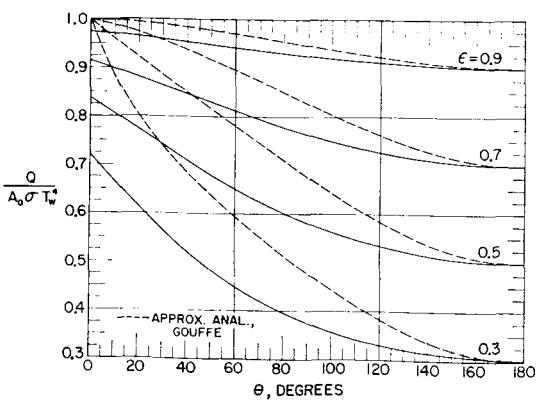

FIG. 2. Efflux of radiation through cavity opening, uniform wall temperature.

whole. The deviation of $Q/A_0\sigma T_w^4$ from ϵ is a measure of the magnitude of the cavity effect. Alternatively, one can interpret the magnitude of $Q/A_0\sigma T_w^4$ as a measure of the emissive power of the cavity opening.

Inspection of Fig. 2 reveals that for any fixed surface emissivity, the deviation of $Q/A_0\sigma T_w^4$ from ϵ grows larger with decreasing values of the cone opening angle. This is in accordance with physical reasoning, since the conical space becomes more "closed-in" at smaller cone angles. Further, it is seen that the cavity effect as just described is much more marked when the surface emissivity is low. For instance, a conical cavity having surface emissivity of 0.3 can achieve a maximum radiant output which is about 72% of that of a black surface. Corresponding gains in emissive power cannot be achieved by the use of cavities when the surfaces involved have high ϵ.

In addition to the solid lines already discussed, there are also shown a set of dashed lines which correspond to the predictions of the highly approximate analysis of Gouffe. In Gouffe's formulation, it was assumed that for each one of a sequence of multireflections within the cavity, the reflected energy was uniformly distributed over

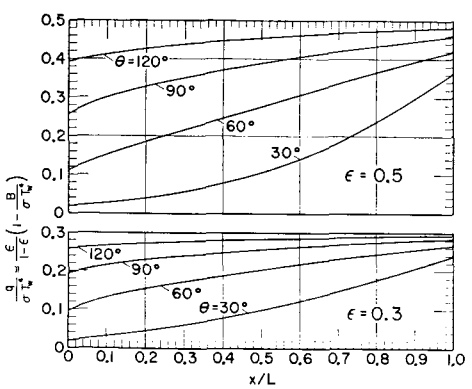

FIG. 3. Surface distribution of heat flux and apparent radiant emittance, uniform wall temperature, $\epsilon=0.3$ and 0.5.

all parts of the cavity wall. Additionally, he employed a highly approximate representation for the fraction of the radiant energy which escaped through the cavity opening during each reflection. It is seen from the figure that there are large deviations between Gouffe's approximate results and those of the present analysis. The largest errors are at small opening angles, i.e., when the cavity effect is most important. However, appreciable errors persist over the full range of opening angles except near $\theta=180°$. It is additionally seen that the errors are greatest for low values of surface emissivity. The comparison shown on Fig. 2 suggests that the Gouffe results for other cavity configurations be regarded with caution.

The numerical solutions of Eq. (5) also provide information on the local radiant energy transport at surface locations within the cavity. This information is presented in Figs. 3, 4, and 5. On the ordinate, there is

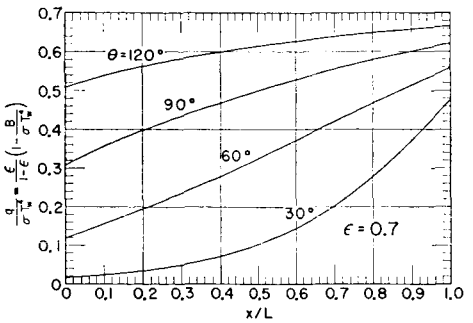

FIG. 4. Surface distribution of heat flux and apparent radiant emittance, uniform wall temperature, $\epsilon=0.7$.

plotted the local heat flux q as well as its equivalent in terms of the apparent radiant emittance B. The abscissa is the position variable x measured along the cavity surface. Figure 3 contains two grids, one for $\epsilon=0.3$ and the second for $\epsilon=0.5$. Figures 4 and 5 correspond, respectively, to $\epsilon=0.7$ and 0.9. Within each figure, curves are plotted for parametric values of opening angle θ.

From the figures, it is seen that for any given θ and ϵ, the local heat flux is always least at the apex of the cone and greatest in the neighborhood of the opening. On the other hand, the apparent radiant emittance of the cavity surface is greatest near the apex and least near the opening. Both these findings appear plausible when it is realized that the incident energy I, which is added to the emission in the B calculation and subtracted from the emission in the q calculation, is largest at the apex. The variation of either q or B along the surface is most marked when the cone opening angle is small and when the surface emissivity is high. It is also easily verified that for a given opening angle θ, the apparent radiant emittance B at any location is higher for surfaces of higher emissivity. Additionally, for a surface of given emissivity, the apparent radiant emittance is higher as the opening angle decreases.

Within the knowledge of the authors, information

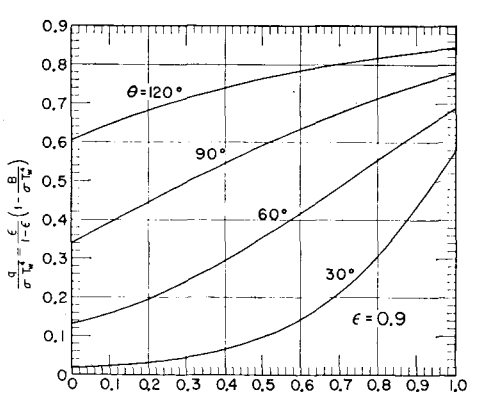

FIG. 5. Surface distribution of heat flux and apparent radiant emittance, uniform wall temperature, $\epsilon=0.9$.

of the type given on Figs. 3, 4, and 5 does not elsewhere appear in the literature and therefore comparisons cannot be made.

Uniform Wall Heat Flux

Corresponding to a uniform heat flux q_w, the radiant flux Q streaming from the cavity may be calculated directly from the first member of Eq. (9) as

$$Q = q_w \pi L^2 \sin(\theta/2). \tag{20}$$

However, since there is no single temperature which characterizes the cavity, one cannot logically define a hemispherical emissivity for the cavity as a whole as was done previously for the case of uniform wall temperature.

The local radiant transport results have been obtained from solutions of Eq. (11) for opening angles θ of 30°, 60°, 90°, and 120°. This information is plotted in Fig. 6 in terms of the local apparent radiant emittance and the local surface temperature. The curves are parametrized by the opening angle. Inspection of the figure reveals that both the apparent radiant emittance and the surface temperature achieve maximum values at the apex and decrease continuously as one proceeds away from the apex. The surface variation of these quantities is accentuated at small opening angles. Additionally, both the apparent radiant emittance and the temperature increase as the opening angle decreases. The apparent radiant emittance is independent of surface emissivity; but the surface temperature is higher for surfaces of lower emissivity. Numerically speaking, the effect of emissivity on the temperature is diminished at small opening angles.

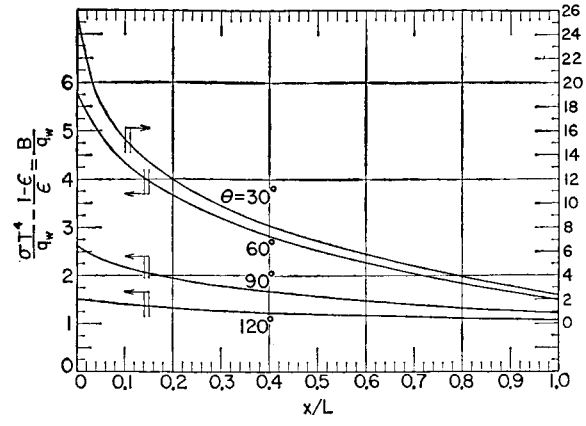

FIG. 6. Surface distribution of temperature and brightness, uniform wall heat flux.

ACKNOWLEDGMENT

This research was sponsored by the National Aeronautics and Space Administration under the technical supervision of Mr. S. Lieblein, Chief, Flow Processes Branch of the NASA Lewis Research Center.